Numerical Simulation of Pulsed Laser Bending

X. R. Zhang

G. Chen[1]

X. Xu[2]

e-mail: xxu@ecn.purdue.edu

School of Mechanical Engineering,
Purdue University,
West Lafayette, IN 47907

The aim of this work is to develop an efficient method for computing pulsed laser bending. During pulsed laser bending, thousands of laser pulses are irradiated onto the target. Simulations of the thermomechanical effect and bending resulted from all the laser pulses would exceed the current computational capability. The method developed in this work requires only several laser pulses to be calculated. Therefore, the computation time is greatly reduced. Using the new method, it is also possible to increase the domain size of calculation and to choose dense meshes to obtain more accurate results. The new method is used to calculate pulsed laser bending of a thin stainless-steel plate. Results calculated for a domain with a reduced size are in good agreement with those obtained by computing all the laser pulses. In addition, experiments of pulsed laser bending are performed. It is found that experimental data and computational results are consistent.
[DOI: 10.1115/1.1459070]

1 Introduction

Laser bending or laser forming is a newly developed, flexible technique which modifies the curvature of sheet metal or hard material using energy of a laser. The schematic of a laser bending process is shown in Fig. 1. The target is irradiated by a focused laser beam passing across the target surface with a certain scanning speed. After laser heating, permanent bending is resulted, with the bending direction toward the laser beam (the positive *z*-direction shown in Fig. 1). Laser bending has been explained by the thermoelastoplastic theory ([1–4]). During the heating period, irradiation of the laser beam produces a sharp temperature gradient in the thickness direction, causing the upper layers of the heated material to expand more than the lower layers. This nonuniform thermal expansion causes the target to bend away from the laser beam. In the meantime, compressive stress and strain are produced by the bulk constraint of the surrounding materials. Because of the high temperature achieved, plastic deformations occur. During cooling, heat flows into the adjacent area and the stress changes from compressive to tensile due to thermal shrinkage. However, the compressive strain generated during heating is not completely cancelled. Therefore, the residual strain in the laser-irradiated area is compressive after the target cools, causing a permanent bending deformation toward the laser beam.

A large amount of experimental and numerical work has been conducted to study CW (continuous wave) laser bending of sheet metals ([5–10]). Applications of laser bending include forming complex shapes and straightening automobile body shells. Laser bending is also being used for high-precision curvature modification during hard disk manufacturing, in which low energy pulsed lasers are used ([4]). Chen et al. [11] studied bending by a line-shape pulsed laser beam using a two-dimensional finite element model. Since the laser beam intensity they used was uniform across the target surface (along the *y*-direction shown in Fig. 1), the effect of bending was calculated using a two-dimensional heat transfer model and a plane-strain model, and the calculation was greatly simplified. Relations between bending angles and pulsed laser parameters were determined by both computational and experimental methods.

Little work has been done on pulsed laser bending using a three-dimensional model. In a common pulsed laser bending operation such as the one used for curvature adjustment in hard disk manufacturing, thermal and thermomechanical phenomena involved are three-dimensional. Laser pulses with Gaussian intensity distributions and high repetition rates are irradiated along the scanning line, as shown in Fig. 2. The main difficulty for simulating pulsed laser bending is that thousands of laser pulses along the laser scanning direction need to be calculated. For example, at a scanning speed of 10 mm/s and a pulse repetition rate of 10 kHz, there will be a total of 2000 pulses irradiated on a 2-mm wide target. Also, the numbers of nodes and elements in a three-dimensional model are much more than that in a two-dimensional model. Direct simulations of any actual pulsed laser bending process are impractical in terms of both the computation time and the computer resource.

In this paper, an efficient calculation method is developed to simulate pulsed laser bending. Instead of calculating bending resulted from all the laser pulses, bending due to a fraction of the total laser pulses is computed. Then, the calculated strain distribution at a cross section perpendicular to the scanning direction is imposed onto the whole target as an initial condition to calculate bending. A computational algorithm is developed. The accuracy of this method is verified by both numerical calculations and experimental measurements.

2 Numerical Procedure

2.1 Calculation of Deformations From the Strain Field

In most pulsed laser bending processes, constant stress and strain fields along the laser scanning direction are obtained. Although a single laser pulse generates nonuniform stress and strain distributions, in practice, laser pulses with same pulse energy, separated by a very small distance compared with the laser beam radius are used. Thus, the laser-induced stress and strain vary little along the scanning direction. With this in mind, it is only necessary to calculate several laser pulses until the stress and strain fields in an *x*-*z* cross-sectional area are not changed by a new laser pulse. Then, the residual strain field in this cross section can be imposed onto the whole domain to calculate the deformation (bending). In other words, a strain field $\{\varepsilon_r\}$, which can be used to calculate displacements of the target after pulsed laser scanning, is generated by calculating only a fraction of the total pulses.

[1]Current address: CNH Global NV, Burr Ridge, IL.

[2]To whom correspondence should be addressed.

Contributed by the Applied Mechanics Division of THE AMERICAN SOCIETY OF MECHANICAL ENGINEERS for publication in the ASME JOURNAL OF APPLIED MECHANICS. Manuscript received by the ASME Applied Mechanics Division, November 9, 2000; final revision, May 8, 2001. Associate Editor: K. T. Ramesh. Discussion on the paper should be addressed to the Editor, Prof. Lewis T. Wheeler, Department of Mechanical Engineering, University of Houston, Houston, TX 77204-4792, and will be accepted until four months after final publication of the paper itself in the ASME JOURNAL OF APPLIED MECHANICS.

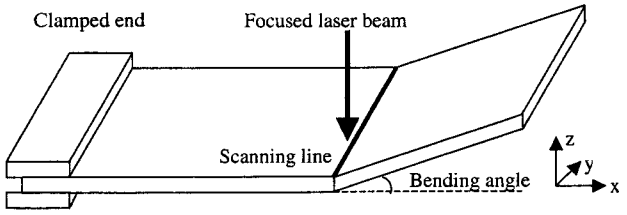

Fig. 1 Schematic of the laser bending process. The laser beam scans along a line in the *y*-direction, causing residual stress and strain in the laser irradiated area and permanent bending.

Before discussing the method of calculating displacements from a strain field, it is worth mentioning that the residual stress field couldn't be used to calculate displacements. The reason is that displacements are dependent not only on the stress but also on the load path when the plastic strain is involved. Different displacements will result from different load paths; even the residual stress fields are the same. On the other hand, there is a one-to-one correspondence between the strain and displacement fields. Therefore, the displacement field of the target can be completely determined by the strain field.

The finite element solver, ABAQUS (HKS, Inc., Pawtucket, RI) is used for the numerical calculation. In ABAQUS, only the stress field can be used as an initial condition for computation. Therefore, an initial stress field, which can produce the strain field equal to the laser produced strain field $\{\varepsilon_r\}$, needs to be obtained first. The method for calculating this stress field is described below.

Consider an undeformed domain without any external forces, but with an initial stress field $\{\sigma_i\}$. In order to satisfy force equilibrium, this initial stress should relax completely. For stress relaxation, the stress field in the domain can be written by

$$\{\sigma\}=\{\sigma_i\}+[E]\{\varepsilon\} \tag{1}$$

where $[E]$ is the matrix of elastic stiffness, $\{\varepsilon\}$ is the strain field due to stress relaxation, and $\{\sigma\}$ is the stress field. After stress relaxation, $\{\sigma\}\rightarrow\{0\}$. The strain field can be obtained by

$$\{\varepsilon\}=-\{\sigma_i\}/[E]. \tag{2}$$

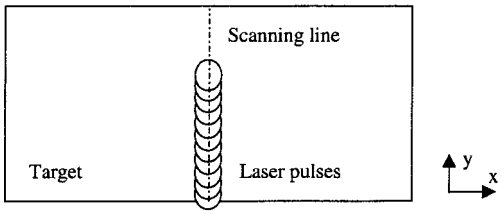

Fig. 2 Irradiation of laser pules on the target surface. The laser scans in the positive *y*-direction.

This equation determines the relationship between an initial stress field and the resulted strain field after stress relaxation. It can be seen that, if an initial stress field $\{\sigma_i\}=-[E]\{\varepsilon_r\}$ is used in the stress relaxation calculation, the resulted strain field will be identical to the strain field $\{\varepsilon_r\}$.

Therefore, in a brief summary, the computation starts with calculating a strain field $\{\varepsilon_r\}$ from several pulses and impose this strain field to the entire domain. Then a stress field $\{\sigma_i\}$ is obtained by computing $-[E]\{\varepsilon_r\}$. This stress field is applied to an undeformed domain followed by a stress relaxation calculation. This calculation yields both the strain $\{\varepsilon_r\}$ as well as the displacement (bending).

To verify this simulation method and use it to compute the pulsed laser bending process, a three-dimensional model is built and simulations of pulsed laser bending are conducted. In the first case, a full-hard 301 stainless steel sample that is 400 μm long, 120 μm wide, and 100 μm thick is irradiated by a pulsed laser. The scanning speed of the laser beam is set to be 195 mm/s, resulting in a total of fourteen pulses along the scanning line; and a 9 μm step size between two adjacent laser pulses. Although the domain size used here is smaller than many of those used in practice, the reduced domain size makes it possible to calculate the temperature, stress, and strain distributions produced by all the 14 laser pulses. On the other hand, to test the new calculation method, the strain distribution in the *x*-*z* cross section at $y=60$ μm after eight laser pulses is imposed onto the whole domain, and the procedures outlined above are used to compute the deformation caused by all the pulses. Results from the two approaches are then compared. In the second case, a full-hard 301 stainless steel sample that is 8 mm long, 1.2 mm wide, and 0.1 mm thick is irradiated by a pulsed laser. The laser scanning speed is also 195 mm/s, resulting in a total of 134 pulses. In this case, only the new method is used since it is impossible to complete the computation of all the 134 pulses within a reasonable amount of time. Experiments are conducted on samples with same dimensions and processing parameters, and the results of experiments and simulations are compared. The laser parameters used in the simulation and the experiment are summarized in Table 1.

The computational domain and mesh for the first case are shown in Fig. 3. Only half of the target is calculated because the central plane is approximated as a symmetry plane. A dense mesh is used around the laser path and then stretched away in length and thickness directions (*x* and *z*-directions). In the dense mesh region, eight elements are used in the *x*-direction, 33 elements in the *z*-direction, and 24 elements in the *y*-direction. A total of 9944 elements are used in the mesh. The same mesh is used for thermal analyses and stress-displacement calculations. The mesh tests are conducted by increasing the mesh density until the calculation result is independent of the mesh density.

Dissipation of energy by the plastic deformation is negligible compared with the high laser energy density during bending. Therefore, it is assumed that the thermal and mechanical problems are decoupled, so that the thermal analysis and the stress and strain calculation can be conducted separately.

Table 1 Pulsed laser parameters

Laser wavelength	1.064 μm
Laser pulse full width	120 ns
Laser pulse repetition	22 kHz
Laser pulse energy	4.4 – 6.4 μJ
Laser beam diameter	50 μm
Laser scanning speed	195 mm/s
Pulse step distance	9 μm

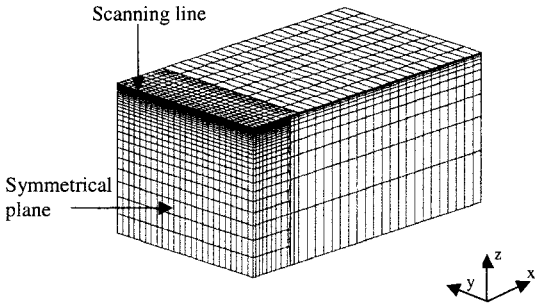

Fig. 3 Computational mesh (x:200 μm, y:120 μm, z:100 μm)

2.2 Thermal Analysis. The thermal analysis is based on solving the three-dimensional heat conduction equation. The initial condition is that the whole specimen is at the room temperature (300 K). Since the left and right boundaries as well as the bottom surface are far away from the laser beam, the boundary conditions at these boundaries are prescribed as the room temperatures. The laser flux is handled as a volumetric heat source absorbed by the target. The laser intensity at the target surface is considered as having a Gaussian distribution in both x and y-directions, which can be expressed as

$$I_s(x,y,t)=I_0(t)\cdot\exp\left(-2\frac{x^2+(y-y_0)^2}{w^2}\right) \tag{3}$$

where $I_0(t)$ is the time-dependent laser intensity at the center of the laser beam ($x=0;y=y_0$) and w is the beam radius. The temporal profile of the laser intensity is treated as increasing linearly from zero to the maximum at 60 ns, then decreasing to zero at the end of the pulse at 120 ns. The local radiation intensity $I(x,y,z,t)$ within the target is calculated considering exponential attenuation and surface reflection as

$$I(x,y,z,t)=(1-R_f)I_s(x,y,t)e^{-\alpha z} \tag{4}$$

where R_f is the optical reflectivity. α is the absorption coefficient given by

$$\alpha=\frac{4\pi\kappa}{\lambda}. \tag{5}$$

The imaginary part of the refractive index κ of stainless steel 301 at the laser wavelength 1.064 μm is unknown, and $\kappa=4.5$ of iron is applied. Properties used in the calculation are considered as temperature-dependent, and are shown in Fig. 4.

Sensitivity of calculated bending with respect to optical reflectivity has been studied ([11]). It was found that a 10% change of optical reflectivity value would cause a 23% difference in the bending angle. Therefore, the uncertainty in reflectivity does influence calculation results significantly. In this work, the reflectivity is measured to be 0.66, which has an uncertainty less than 5%.

The thermal analysis is carried out for laser pulse energy of 4.4 μJ, 5.4 μJ, and 6.4 μJ, respectively. The maximum temperatures obtained are all lower than the melting point of steel (1650 K).

2.3 Stress and Strain Calculation. For each laser pulse, the transient temperature field obtained from the thermal analysis is used as thermal loading, and residual stress and strain fields of the previous pulse are input as initial conditions to solve the quasi-static force equilibrium equations. The material is assumed to be linearly elastic-perfectly plastic. The Von Mises yield criterion is used to model the onset of plasticity. The boundary conditions are zero displacement in the x-direction and no rotations around y and z-axes in the symmetry plane, and all other surfaces are stress free. Details of the equations to be solved have been described elsewhere ([10]).

As shown in Fig. 4, material properties including density, yield stress, and Young's modulus are considered temperature-dependent. However, the strain rate enhancement effect is neglected because temperature-dependent data are unavailable. A constant value (0.3) of Poisson's ratio is used. Sensitivity of unknown material properties on the computational results has been studied ([11]). It was found that possible errors resulting from extrapolating material properties at high temperatures and using a constant Poisson's ratio were within a few percent.

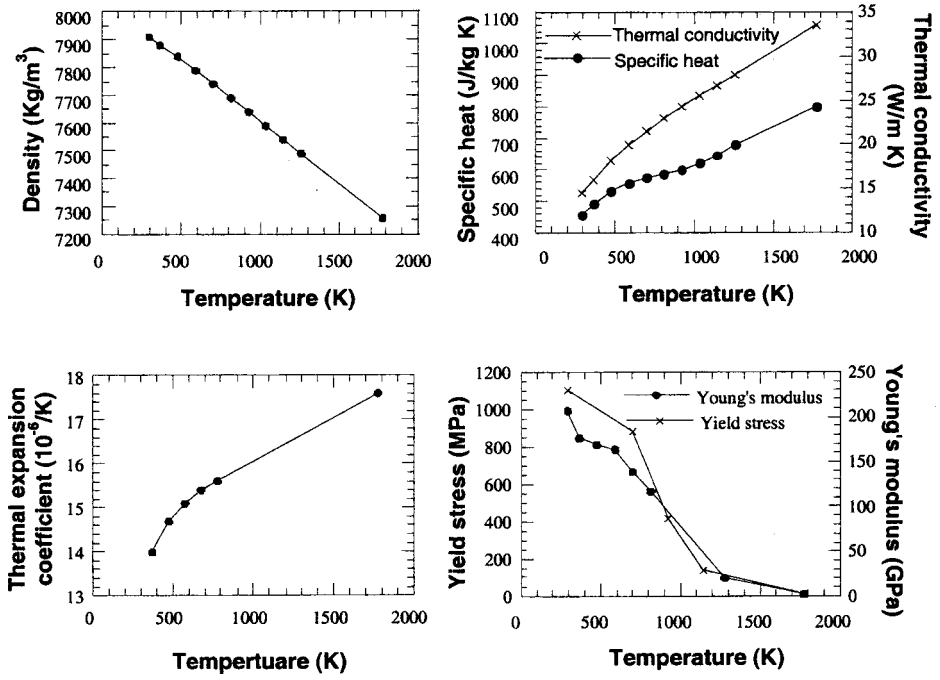

Fig. 4 Thermal and mechanical properties of full-hard 301 stainless steel

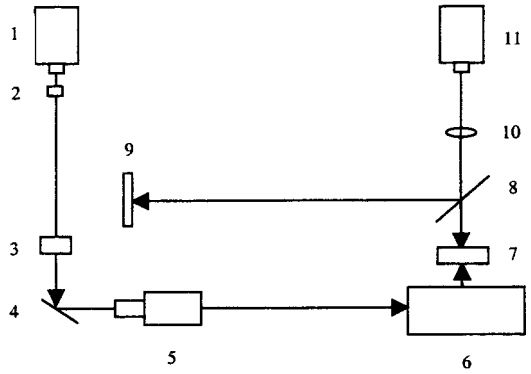

Fig. 5 Experimental setup for pulsed laser bending and for measuring the bending angle [1–ND:VA laser, 2–shutter, 3–polarizing beam splitter, 4–mirror, 5–beam expander, 6–X&Y scanner, 7–specimen, 8–beam splitter, 9–position-sensitive detector, 10–lens, 11–He-Ne laser]

3 Experimental Measurements

Experiments of bending of stainless steel are performed to verify the calculation results. The laser used in experiments is a pulsed Nd:VA laser with the same operation parameters shown in Table 1. Figure 5 illustrates the experimental setup for performing pulsed laser bending as well as for measuring the bending angle. The Nd:VA laser beam scans the specimen surface along the *y*-axis (Fig. 1) at a speed of 195 mm/s. The scanning speed is accurately controlled by a digital scanning system and the pulse step is 9 μm at this speed. An He-Ne laser beam is focused at the free end of the target to measure the bending angle in the *z*-direction. The reflected He-Ne laser beam is received by a position sensitive detector (PSD) with 1-μm sensitivity in position measurements. The accuracy of the bending angle measurement is about ± 1.5 μrad when the distance between the specimen and the PSD is set to 750 mm in the experiment. After laser scanning, the target bends toward the laser beam, causing the reflected He-Ne laser beam to move across the PSD. The position change of He-Ne laser beam can be converted to the bending angle of the specimen using geometrical calculations. The whole apparatus is set on a vibration-isolation table. Polished full hard 301 stainless steel sheets are used as targets.

4 Results and Discussion

Results calculated using a reduced domain size are presented to illustrate the temperature and residual strain and stress distributions induced by laser pulses. Bending deformations obtained by the new calculation method and by computing all laser pulses are then compared. Bending deformations resulted from different laser pulse energy are also presented. For the second case for which a larger sample is used, the calculated bending angles using the new method are compared with the experimental data.

4.1 Results Calculated Using a Reduced Domain Size Temperature distributions along *x* and *y*-directions and at different times are shown in Fig. 6. The laser pulse energy is 5.4 μJ and the pulse center is located at $y=54$ μm. Figure 6(*a*) shows the temperature distribution along the scanning line (the *y*-direction). It can be seen that the maximum temperature, $T_{\max}$, is reached at the pulse center. $T_{\max}$ increases once the laser pulse is irradiated on the surface and reaches its peak value 988.1 K at 87.7 ns, and then drops slowly to 365.5 K at 2.2 μs. It can be estimated that the laser-heated region is around 30 μm in radius. Figure 6(*b*) is the temperature distribution along the depth direction (the *z*-direction), beginning from the upper surface of the target. The maximum temperature is obtained at the upper surface and reaches 988.1 K at $t=87.7$ ns. The heat propagation depth is

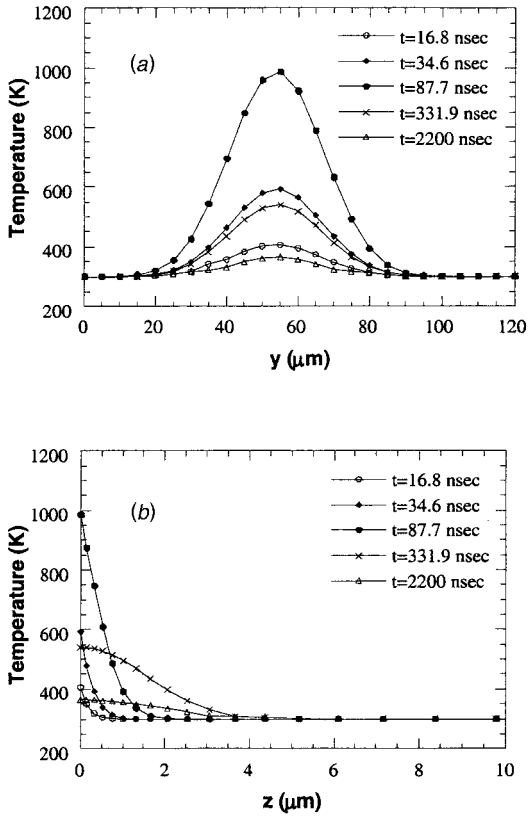

Fig. 6 Temperature distributions induced by the seventh pulse (pulse energy 5.4 μJ; pulse center at $y=54$ μm) (*a*) along the scanning line, (*b*) along the *z*-direction

around 4 μm at 2.2 μs and the temperature gradient during heating period is as high as 350 K/μm. This sharp temperature gradient causes nonuniform plastic strains in the target and the permanent bending deformation after laser heating.

Residual strain ε_{xx} and stress σ_{xx} distributions along the laser scanning path obtained from calculating all the fourteen pulses are plotted in Fig. 7(*a*) and Fig. 7(*b*), respectively. Only the components ε_{xx} and σ_{xx} are plotted since they are more important to the bending deformation than other components. It can be seen from Fig. 7(*a*) that after four pulses, the strain field in regions about 15 μm behind the new laser pulse is no longer changed. In other words, in the *y*-direction, each pulse only affects the stress and strain field within 15 μm from its center. It is also seen that after the laser pulses pass the whole target width, the residual stress and strain fields of the target are independent of the *y*-coordinate with the exception near the two edges, which is caused by the free stress boundary conditions. The uniform stress and strain along the *y*-direction are consistent with the assumption used in the calculation.

Residual strain ε_{xx} and stress σ_{xx} distributions along the *x*-direction at the upper surface are shown in Fig. 8(*a*) and Fig. 8(*b*), respectively. They are obtained after eight laser pulses in the cross section $y=60$ μm. It can be seen from Fig. 8(*a*) that the strain ε_{xx} is compressive within 15 μm from the center of the laser pulse. This agrees with the theoretical prediction that the compressive residual strain will be obtained near the center of laser-irradiated area where the temperature is the highest and the plastic deformation occurs ([4]). The residual strain ε_{xx} becomes positive (tensile strain) at locations more than 15 μm away from the center. The tensile strain in this region is due to the tensile force produced by thermal shrinkage during cooling. The total strained region is about 30 μm from the center of the laser beam and is slightly larger than the radius of the laser beam (25 μm). In

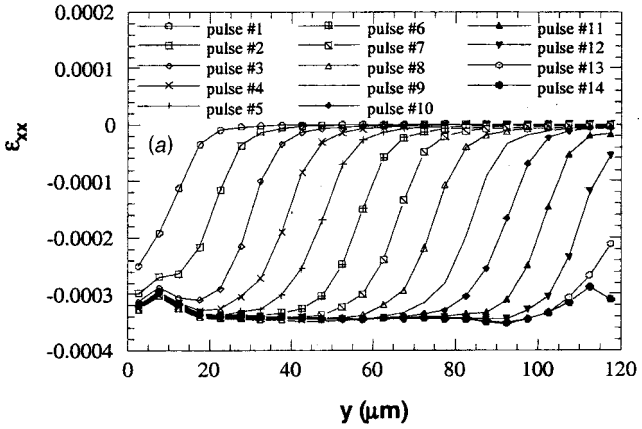

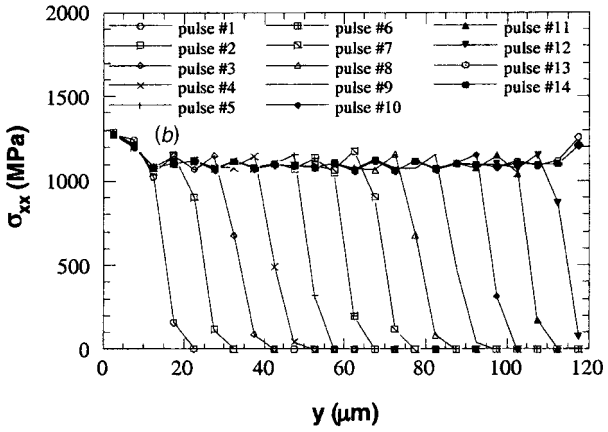

Fig. 7 (*a*) Residual strain (ε_{xx}), (*b*) residual stress (σ_{xx}) distributions along the scanning line induced by each laser pulse (pulse energy 5.4 μJ; scanning speed 195 mm/s)

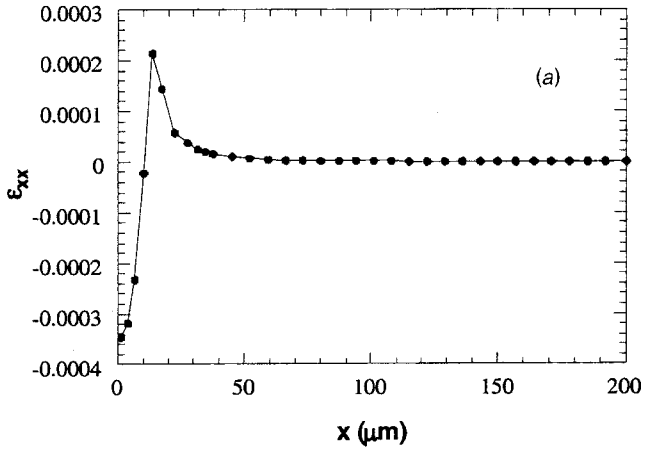

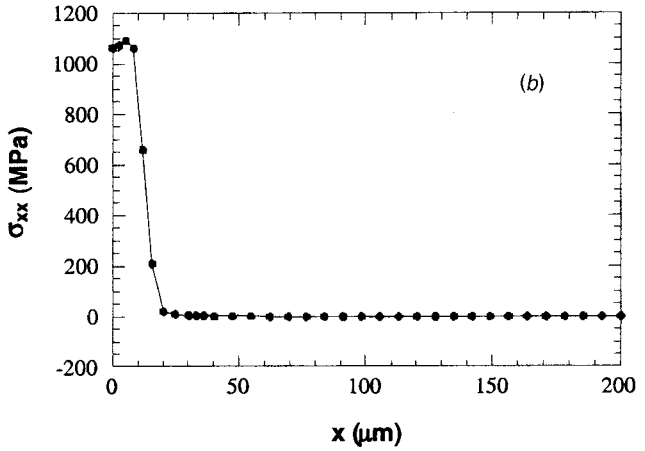

Fig. 8 (*a*) Residual strain (ε_{xx}), (*b*) residual stress (σ_{xx}) distributions along the *x*-direction ($y=60$ μm and $z=0$ μm) after eight pulses

Fig. 8(*b*), the stress σ_{xx} is tensile and its value is around 1.1 GPa in the region within 15 μm from the pulse center. This large tensile stress cancels more than 90% of the plastic strain produced during heating in this region. The tensile stress drops quickly to zero at about 25 μm from the center of the laser beam.

The strain distribution ε_{xx} calculated from the initial stress field $\{\sigma_i\}$ using the new simulation method is shown in Fig. 9. The average value of ε_{xx} obtained from the new method is -3.47×10^{-4}, comparing with the value of -3.42×10^{-4} calculated from all the 14 pulses. The two strain values are in very good agreement except at two edges. Again, the difference is caused by the free boundary conditions at the edges.

The off-plane displacement w is of prime interest since it reflects the amount of bending. The comparison between the deformation calculated from the initial stress $\{\sigma_i\}$ and that obtained by calculating all the pulses is shown in Fig. 10. Results at the cross section $y=60$ μm are plotted. It can be seen that displacements w of the two approaches are consistent and the bending angles are almost identical. The difference between the two curves is located around the transition mesh region. This is because that the element size and the shape in the transition region are not all the same, and errors are produced when the residual strain of one x-z cross section is imposed to the whole domain. It is seen from Fig. 10 that a "V" shape surface deformation is resulted after laser scanning, with the valley located at around 10 μm from the center of the scanning line. The positive off-plane displacement near the center of the scanning line is produced by thermal expansion along the positive z-direction because of the free-surface boundary condition.

Figure 11 shows the off-plane displacement w of the central point on the free edge of the surface ($x=200$ μm,$y=60$ μm,$z=100$ μm) produced after each laser pulse with pulse energy of 4.4 μJ, 5.4 μJ, and 6.4 μJ, respectively. As expected, laser pulses with high energy produce more bending. It is also seen that w increases almost linearly with the number of pulses for all the three cases.

4.2 Comparison Between Experimental and Numerical Results. Bending angles obtained experimentally are compared with calculated values as shown in Fig. 12. Laser energy of 4.4 μJ, 5.4 μJ, and 6.4 μJ is used in the experiment. On the other hand, calculations are carried out using the new method, in which the strain distribution obtained after eight laser pulses is imposed onto the entire computation domain. The size of the computation domain is 0.2 mm$\times$1.2 mm$\times$0.1 mm, which is identical to the sample size used in the experiment in the y and z-directions. Using a smaller size in the x-direction does not affect the computation results, since regions at x greater than 0.2 mm undergo a rigid rotation only. From the figure, it is seen that the experimental results agree with the calculated values within the experimental uncertainty. Both the experiment and simulation show the bending angle increases almost linearly with the pulse energy.

The agreements between the results of two numerical methods, and between the experimental and numerical results show that the

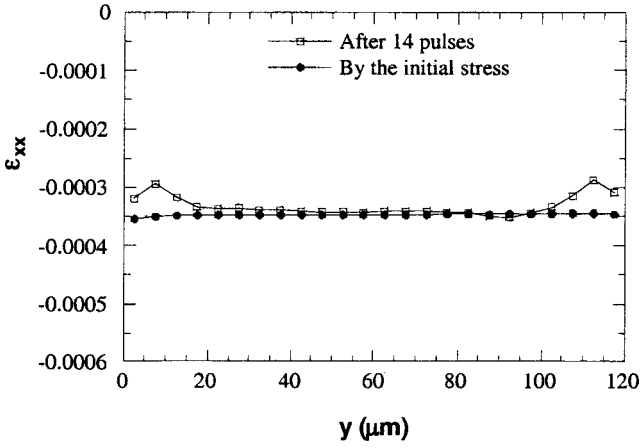

Fig. 9 Residual strain ε_{xx} along the scanning line on the top surface obtained by calculating all the 14 pulses and by using the new method (pulse energy 5.4 μJ; scanning speed 195 mm/s)

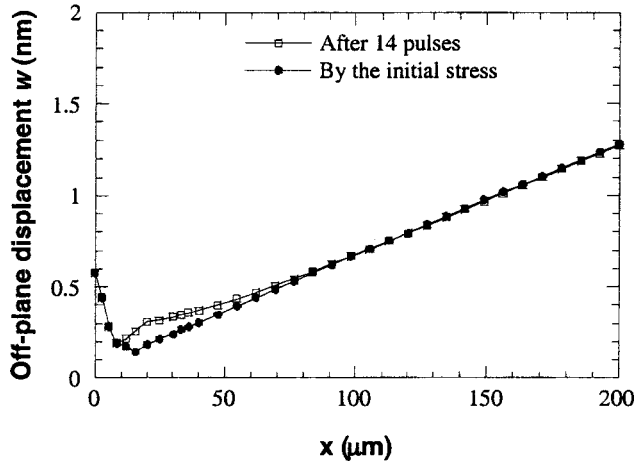

Fig. 10 Displacement w along the x-direction ($y=60$ μm and $z=0$ μm) obtained by calculating all the laser pulses and by using the new method (pulse energy 5.4 μJ; scanning speed 195 mm/s)

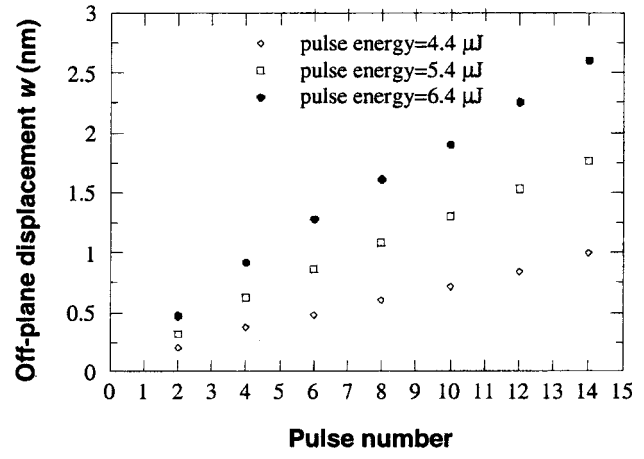

Fig. 11 Calculated displacement w at the free edge after each laser pulse as a function of laser energy

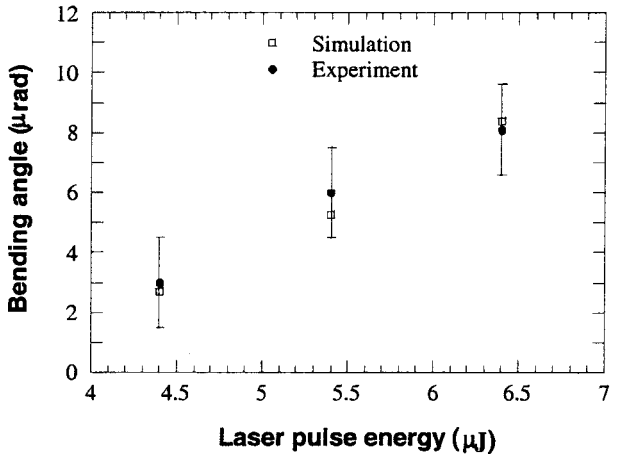

Fig. 12 Comparison between the measured bending angles and the simulation results obtained using the new method

newly developed method is indeed capable of computing pulsed laser bending. As indicated previously, the advantage of the new method is that the computation time is greatly reduced. For each laser pulse in the first case, about two hours are needed for the temperature calculation and four hours for the stress calculation using an 800 MHz Dell PC Workstation. It takes about 84 hours to obtain the bending deformation resulted from all the 14 pulses, and 50 hours when the new method is used. On the other hand, for the second case, it would have taken more than 10,000 hours to obtain the bending deformation if all the pulses were to be calculated. Using the new method, it only takes about 100 hours to complete the calculation. Thus, even for a sample as small as a few mm in size, bending can only be calculated with the use of the new method.

One concern of using the new method for calculating pulsed laser bending is when the laser beam scans the surface at a very high speed, thus the pulse step-size becomes large enough to cause nonuniform stress and strain along the scanning line. However, if the laser-induced stress and strain distribution is periodic, i.e., produced by high-speed scanning of the laser beam with constant energy per pulse, this method still works. The strain distribution within a period along the y-direction can be imposed to the whole domain, and the remaining steps follow those described previously in Section 2.1.

5 Conclusion

A new efficient method for computing pulsed laser bending is developed. The total computation time is greatly reduced and results are found to agree with those obtained using a conventional computation method. Experimental studies are also carried out to verify the simulation results. It is found that the calculated results agree with the experimental values. For most pulsed laser bending processes, the newly developed method is the only possible way to compute bending within a reasonable amount of time.

Acknowledgment

Support to this work by the National Science Foundation (DMI-9908176) is gratefully acknowledged. The authors also thank Dr. Andrew C. Tam of IBM Almaden Research Center for collaborations on this work.

References

[1] Namba, Y., 1986, "Laser Forming in Space," *International Conference on Lasers*, C. P. Wang et al., eds., STS Press, Las Vegas, NV, pp. 403–407.
[2] Geiger, M., and Vollertsen, F., 1993, "The Mechanisms of Laser Forming," Ann. CIRP, **42**, pp. 301–304.
[3] Vollertsen, F., 1994, "Mechanisms and Models for Laser Forming," *Laser Assisted Net Shape Engineering, Proc. of the LANE*, Vol. 1, M. Geiger et al., eds., Meisenbach, Bamberg, Germany, pp. 345–360.

[4] Chen, G., Xu, X., Poon, C. C., and Tam, A. C., 1998, ''Laser-Assisted Microscale Deformation of Stainless Steels and Ceramics,'' Opt. Eng., **37**, pp. 2837–2842.
[5] Scully, K., 1987, ''Laser Line Heating,'' J. Ship Res., **3**, pp. 237–246.
[6] Alberti, N., Fratini, L., and Micari, F., 1994, ''Numerical Simulation of the Laser Bending Processing by a Coupled Thermal Mechanical Analysis,'' *Laser Assisted Net Shape Engineering, Proc. of the LANE*, Vol. 1, M. Geiger et al., eds., Meisenbach, Bamberg, Germany, pp. 327–336.
[7] Pridham, M., and Thomson, G., 1995, ''An Investigation of Laser Forming Using Empirical Methods and Finite Element Analysis,'' J. Des. Manufact., **5**, pp. 203–211.
[8] Magee, J., Watkins, K. G., and Steen, W. M., 1997, ''Laser Forming of Aerospace Alloys,'' *Proc. of Laser Institute of America, ICALEO*, **83**, Laser Institute of America, Orlando, FL, pp. 156–165.
[9] Hsiao, Y. C., Shimizu, H., Firth, L., Maher, W., and Masubuchi, K., 1997, ''Finite Element Modeling of Laser Forming,'' *Proc. of Laser Institute of America, ICALEO*, **83**, Laser Institute of America, Orlando, FL, pp. 31–40.
[10] Chen, G., and Xu, X., 2000, ''3D CW Laser Forming of Thin Stainless Steel Sheets,'' ASME J. Manuf. Sci. Eng., in press.
[11] Chen, G., Xu, X., Poon, C. C., and Tam, A. C., 1999, ''Experimental and Numerical Studies on Microscale Bending of Stainless Steel With Pulsed Laser,'' ASME J. Appl. Mech., **66**, pp. 772–779.